Dynamics of infrared-to-visible upconversion in $Cs_3Lu_2Br_9$:1%Er^{3+}

Markus P. Hehlen,* Gabriela Frei, and Hans U. Güdel
Institut für Anorganische Chemie, Universität Bern, Freiestrasse 3, 3000 Bern 9, Switzerland
(Received 26 April 1994)

Single crystals of $Cs_3Lu_2Br_9$:1%Er^{3+} were grown using the Bridgman technique. The low phonon energy of ≤ 190 cm^{-1} strongly suppresses multiphonon relaxation in this host. For a series of excited states radiative relaxation is found to be dominant. As a consequence, $Cs_3Lu_2Br_9$:1%Er^{3+} shows strong visible upconversion luminescence from $^2H_{9/2}$ and $^4F_{7/2}$ when excited into the $^4I_{9/2}$ and $^4I_{11/2}$ multiplets in the near infrared, respectively. The upconversion dynamics for both excitations was studied in detail using time-resolved spectroscopy. Both excited-state absorption (ESA) and energy-transfer upconversion (ETU) were found to be active and could be identified on the basis of the upconversion transients. For the population of the $^4F_{7/2}$ and $^4S_{3/2}$ states both ESA and ETU can be observed simultaneously. The relative efficiency of ESA and ETU is determined by the energetic resonance of the respective processes. Whereas nonresonant ESA during the 10 ns laser pulse is strongly suppressed for energy mismatches > 12 cm^{-1}, ETU is still efficient. An analysis of the upconversion transients shows that energy migration is dominant even at 1% Er^{3+} dotation. The excitations have excitonic character leading to a characteristic prolongation of the decays in the upconversion transients.

I. INTRODUCTION

The ternary rare-earth halides K_2LaX_5 and $Cs_3Lu_2X_9$ (X=Cl, Br, I) doped with Er^{3+} or Tm^{3+} show intense visible (VIS) luminescence when excited in the near infrared (NIR).[1,2] The luminescence mainly occurs from states which are efficiently quenched in oxide and fluoride host lattices. This is due to the very low phonon energies in chloride, bromide, and iodide systems which strongly suppress multiphonon relaxation for most of the excited states. As a variety of states is being populated during the upconversion processes excited-state dynamics are expected to be very different from the high-phonon oxide and fluoride hosts. This has been demonstrated for $CsCdBr_3$:Er^{3+} in which several upconversion processes could be studied in detail.[3]

In the present paper we report on the upconversion dynamics of $Cs_3Lu_2Br_9$:1%Er^{3+}. Besides multiphonon relaxation processes, numerous energy migration and cross-relaxation processes active in the concentrated $Cs_3Er_2Br_9$ are expected to be suppressed in this diluted system.[4] Therefore, the number of competing nonradiative processes is reduced and specific mechanisms can be studied in detail. On the basis of a complete crystal-field analysis of $Cs_3Lu_2Br_9$:1%Er^{3+},[5] the temporal behavior and the efficiency of different upconversion mechanisms can be directly correlated with their energetic resonance. $Cs_3Lu_2Br_9$:1%Er^{3+} therefore represents an ideal system to gain insight into the basic processes leading to upconversion.

II. EXPERIMENT

Dry MBr_3 (M=Lu^{3+},Er^{3+}) and CsBr were prepared following the procedures given in Ref. 2. Crystals of $Cs_3Lu_2Br_9$:1%Er^{3+} were grown in silica ampoules using the Bridgman technique.[6] Polarized absorption spectra were recorded on a Cary 5E (Varian) spectrometer.

Continuous-wave upconversion luminescence measurements were performed using an argon-ion laser (Spectra Physics 2045) pumped Ti:sapphire laser (Schwartz Electrooptics) in standing-wave configuration. The sample luminescence was dispersed by a 0.85-m double monochromator (Spex 1402) using 500-nm blazed 1200 grooves/mm gratings and detected by a cooled photomultiplier (RCA 31034) using a photon counting system (Stanford Research 400).

For pulsed upconversion luminescence measurements the output of a Nd:YAG laser (Quanta Ray DCR-3, 20 Hz, frequency doubled) pumped dye laser (Lambda Physik FL3002) was Raman shifted (Quanta Ray RS-1; H_2, 240 psi). Near-infrared excitation at 802 and 980 nm was provided using the dyes Rhodamine B and Pyridine 1 in methanol, respectively. The sample luminescence was dispersed by a 0.75-m single monochromator (Spex 1702) using 500-nm blazed 600 grooves/mm gratings and detected as described above. For the time-resolved measurements a multichannel scaler (Stanford Research SR430) was used. Sample cooling was achieved using the helium-gas flow technique for the laser experiments or a closed-cycle cryostat (Air Products Displex) for the absorption measurements.[6]

III. MODELS FOR ENERGY TRANSFER UPCONVERSION

Several processes are known to lead to the population of highly excited states after excitation in the near infrared.[7,8] Most of the processes rely either on an excited-state absorption (ESA) or an energy-transfer upconversion (ETU). In this section basic aspects of ETU are discussed. The ETU process, in which an excited ion nonradiatively transfers its energy to an already excited neighboring ion, is one of the most efficient upconversion

mechanisms. ETU has been observed in a variety of systems, and in most of these it is the dominant process.[9] The energy transfer can arise from both electric multipole or exchange interactions, and its rate constant is strongly dependent on the ion-ion separation.[10] The crystallographic structure of the system and the dopant concentration determine the number as well as the nature of the ion pairs which are formed in the host lattice. Trivalent metal ions doped in low concentrations in lattices such as $CsCdBr_3$, $CsMgBr_3$, or $CsMgCl_3$ predominantly enter as well-defined M^{3+}-vacancy-M^{3+} ion pairs.[11] These lattices therefore offer isolated units for two-ion ETU. This is different in lattices where the active ions are doped statistically. There is a distribution of single ions, ion pairs, and higher clusters, and at higher dopant levels the excitation energy can efficiently migrate through the lattice.[8] Compared to the isolated ion pairs described above, different excited-state dynamics are expected for ions which participate in energy migration. The dynamic properties of ETU for both cases, an isolated ion pair and an energy-migration system, are discussed below.

A. Isolated ion pair model

Figure 1(a) schematically shows the relaxation processes of an isolated pair of ions with equal energy spacing between the states $|1\rangle$, $|2\rangle$, and $|3\rangle$. After excitation of both ions to state $|2\rangle$ several relaxation processes can take place: State $|3\rangle$ on one ion can be populated with a rate constant W_t by a nonradiative energy transfer from its partner; this is the ETU process which leads to upconversion luminescence from state $|3\rangle$. Once excited, both ions can individually relax from $|2\rangle$ to $|1\rangle$ with a rate constant W_2. State $|3\rangle$ can in principle relax to both states $|2\rangle$ and $|1\rangle$. In Fig. 1(a) this branching of $|3\rangle$ is not shown, the reason being that the ion pair is assumed isolated. After ETU on an isolated ion pair, one ion is in state $|1\rangle$ and its partner is in state $|3\rangle$. Populating state $|2\rangle$ in a subsequent relaxation from state $|3\rangle$ does not lead to a situation from which a further ETU process could take place and therefore does not influence population $|3\rangle$ any more. Thus only the *total* relaxation from state $|3\rangle$ and not its branching is relevant for the temporal behavior of population N_3. For this reason, the description of the system in terms of the single-ion states $|1\rangle$, $|2\rangle$, and $|3\rangle$ is not adequate, rather the states of the ion pair have to be considered. The temporal behavior of the population N_3 after exciting both ions to $|2\rangle$ can be solved analytically and is described by

$$N_3(t)=\frac{N_d^0 W_t}{W_3-(2W_2+W_t)}\times\{e^{-(2W_2+W_t)t}-e^{-W_3 t}\}\ , \tag{1}$$

where N_d^0 is the initial population of doubly excited ion pairs.[12] The relative magnitude of the two exponents in Eq. (1) determines the shape of the transient $N_3(t)$, which contains a rise and a decay part. In Eq. (1) we note the multiplication of the rate constant W_2 by a factor of 2. This is because the initial state for the ETU process decays with W_2 on *both* ions. Equation (1) was used for the analysis of the upconversion dynamics in $CsCdBr_3$:Er^{3+} (Ref. 3) and CaF_2:Pr^{3+} (Ref. 12) where the relaxation of isolated ion pairs was found to be an adequate model for ETU.

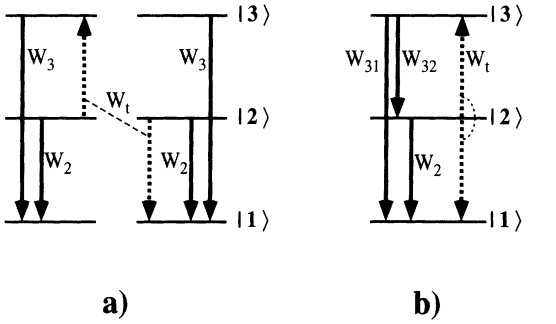

FIG. 1. Schematic representation of the relaxation processes (a) on an isolated ion pair and (b) on an ion participating in energy migration. Radiative and nonradiative processes are represented by solid and dashed arrows, respectively. The processes and rate constants are described in Sec. III.

B. Energy migration model

We now consider the same model as described above but in addition introduce energy migration within state $|2\rangle$ [see Fig. 1(b)]. The rate constant for energy migration is assumed to be infinite and thus not included explicitly. For this reason, the excitation $|2\rangle$ is no longer localized but has an excitonic character. Due to this delocalization, one ion is representative for the average excited-state populations N_1, N_2, N_3 of all the ions in the lattice. In contrast to the isolated ion pair model described above, this system can therefore be described in terms of the single-ion states $|1\rangle$, $|2\rangle$, and $|3\rangle$. The temporal behavior is described by three coupled nonlinear differential equations:

$$\begin{aligned}
\partial N_3/\partial t &= W_t N_2^2-(W_{31}+W_{32})N_3\ ,\\
\partial N_2/\partial t &= -2W_t N_2^2-W_2 N_2+W_{32}N_3\ ,\\
\partial N_1/\partial t &= W_t N_2^2+W_2 N_2+W_{31}N_3\ .
\end{aligned} \tag{2}$$

These equations cannot be solved analytically and have to be integrated using numerical techniques. In a highly doped host lattice where energy migration is dominant, Eqs. (2) provide the adequate description and lead to two major differences compared to the isolated ion pair model Eq. (1): (i) The initial state $|2\rangle$ for ETU decays with a rate constant of *only* W_2. (ii) The branching of state $|3\rangle$ is essential and has therefore been included in Fig. 1(b). As N_2 represents an equilibrium population for state $|2\rangle$ of all the ions in the lattice, the relaxation $|3\rangle\rightarrow|2\rangle$ provides a recycling of population which can again be upconverted to state $|3\rangle$. In contrast to the isolated ion pair model, the branching of state $|3\rangle$ therefore affects the excited-state dynamics.

Figure 2 shows upconversion transients for both models calculated using the same values for the rate constants

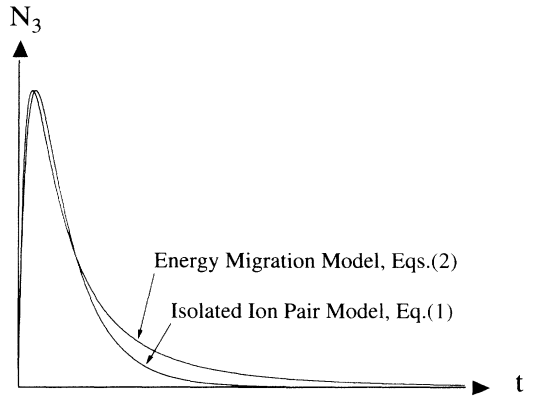

FIG. 2. Calculated upconversion transients for both the isolated ion pair Eq. (1) and the energy-migration model Eqs. (2). The values for the rate constants are the same for both models, $W_2=100\ s^{-1}$, $W_3=5000\ s^{-1}$, and $W_t=1000\ s^{-1}$, for the branching $W_{32}=W_3$ and $W_{31}=0$ was assumed.

W_2, W_3, and W_t. For simplicity $W_{32}=W_3$ and $W_{31}=0$ was assumed, and therefore the difference of the model curves is only due to the different relaxation of the ETU initial state $|2\rangle$. Whereas the two upconversion transients $N_3(t)$ have a very similar rise time, energy migration leads to a pronounced prolongation of the decay time. Time-resolved upconversion spectroscopy should therefore be able to distinguish between processes on isolated ion pairs and those in extended coupled systems.

IV. RESULTS

Figure 3 shows the σ-polarized absorption spectrum of $Cs_3Lu_2Br_9$:1%Er^{3+} at 15 K in the NIR and VIS spectral region. The multiplets are readily assigned as shown in the figure. The insets show the two transitions $^4I_{15/2}\rightarrow{}^4I_{11/2}$ and $^4I_{15/2}\rightarrow{}^4I_{9/2}$ which were used to excite upconversion luminescence. The labels $^4I_{11/2}(0'\ldots5')$ and $^4I_{9/2}(0'\ldots4')$ denote crystal-field levels and were assigned on the basis of polarized absorption measurements[5] (see Table I).

Figure 4 presents unpolarized upconversion luminescence spectra of $Cs_3Lu_2Br_9$:1%Er^{3+} and $Cs_3Er_2Br_9$ at room temperature using continuous-wave (CW) excitation of $^4I_{11/2}$. Whereas luminescence from $^4F_{7/2}$ dominates the $Cs_3Lu_2Br_9$:1%Er^{3+} spectrum, the intensity distribution is completely different in $Cs_3Er_2Br_9$ and shifted towards lower energy.

Unpolarized upconversion luminescence spectra of $Cs_3Lu_2Br_9$:1%Er^{3+} at 10 K using pulsed excitation of $^4I_{11/2}$ and $^4I_{9/2}$ are shown in Fig. 5. Corresponding spectra using CW excitation look very similar. The intensity distribution of the two spectra in Fig. 5 is very different. Whereas exciting $^4I_{11/2}$ predominantly leads to $^4F_{7/2}$ luminescence, $^4I_{9/2}$ excitation mainly results in $^2H_{9/2}$ and weak $^4S_{3/2}$ luminescence.

Figure 6 shows an unpolarized upconversion excitation spectrum of $Cs_3Lu_2Br_9$:1%Er^{3+} exciting the $^4I_{15/2}\rightarrow{}^4I_{11/2}$ transitions at 10 K and monitoring the $^4F_{7/2}\rightarrow{}^4I_{15/2}$ luminescence. Besides the crystal-field transitions $^4I_{15/2}(0)\rightarrow{}^4I_{11/2}(0'\ldots5')$ (see Table I) two significantly broader bands I and II are observed.

The upconversion transients of $^2H_{9/2}$ and $^4S_{3/2}$ obtained under pulsed $^4I_{9/2}$ excitation of $Cs_3Lu_2Br_9$:1%Er^{3+} at 10 K are shown in Figs. 7(a) and 7(b), respectively. No luminescence intensity at $t=0$ is observed for $^2H_{9/2}$, the transient exhibits a typical rise and decay part [Fig. 7(a)]. The $^4S_{3/2}$ transient, in contrast, has an instantaneous rise, and the decay is characterized by two separate rate constants [Fig. 7(b)].

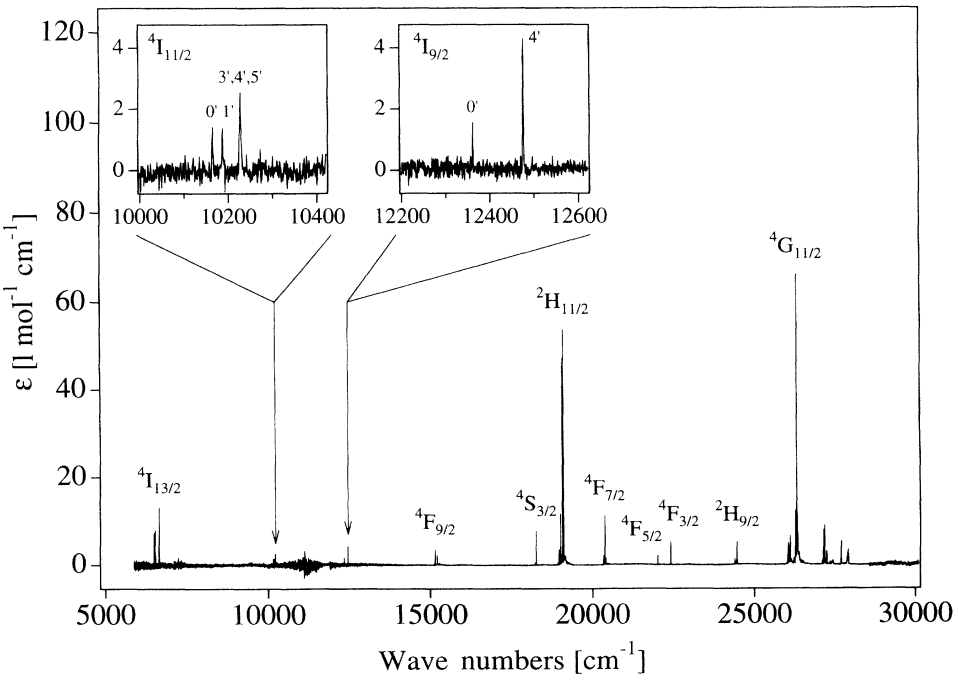

FIG. 3. σ-polarized absorption spectrum of $Cs_3Lu_2Br_9$:1%Er^{3+} at 15 K. The insets show the states $^4I_{11/2}$ and $^4I_{9/2}$ which were used for the excitation of visible upconversion luminescence. For $^4I_{11/2}$ and $^4I_{9/2}$ the assignment to crystal-field levels is given based on Ref. 5 (see Table I).

TABLE I. Experimentally determined crystal-field energies in $Cs_3Lu_2Br_9$:1%Er^{3+} taken from Ref. 5. Only the multiplets relevant for the discussion are shown.

State	Energy (cm^{-1})	State	Energy (cm^{-1})
$^4I_{15/2}(0)$	0	$^4I_{9/2}(0')$	12 361
(1)	42	(1')	12 384
(2)	78	(2')	12 426
(3)	81	(3')	. . .
(4)	90	(4')	12 476
(5)	236		
(6)	241	$^4S_{3/2}(0')$	18 251
(7)	246	(1')	18 278
$^4I_{13/2}(0')$	6 499	$^4F_{7/2}(0')$	20 346
(1')	6 538	(1')	20 386
(2')	6 551	(2')	20 413
(3')	6 560	(3')	. . .
(4')	6 659		
(5')	6 661	$^2H_{9/2}(0')$	24 402
(6')	6 662	(1')	24 410
		(2')	24 433
$^4I_{11/2}(0')$	10 164	(3')	24 465
(1')	10 187	(4')	24 471
(2')	. . .		
(3')	10 225		
(4')	10 227		
(5')	10 228		

Figure 8 shows upconversion transients of $^4F_{7/2}$ on a logarithmic ordinate scale obtained exciting different $^4I_{11/2}$ crystal-field levels (see Fig. 6). Depending on the excitation energy (A,B,C), different $^4F_{7/2}$ temporal behavior is found. Whereas transient A has the slowest rise (see inset) and decay constants, transient B has maximum intensity at $t=0$ (see inset) and decays fast with a decay time constant of about 270 μs.

V. DISCUSSION

A. Upconversion luminescence in $Cs_3Lu_2Br_9$:1%Er^{3+}

The ternary rare-earth halides $Cs_3Er_2X_9$ (X=Cl,Br,I) and their diluted analogs exhibit efficient upconversion luminescence in the green, blue and UV spectral regions when excited in the near infrared (NIR).[2,4] As indicated in Fig. 3 both multiplets $^4I_{11/2}$ and $^4I_{9/2}$ can be used for excitation of VIS luminescence.

In $Cs_3Lu_2Br_9$:1%Er^{3+} each $|SLJ\rangle$ multiplet is split by the C_{3v} crystal field into $\frac{1}{2}(2J+1)$ Kramers doublets. The insets of Fig. 3 as well as Fig. 6 show some of the crystal-field transitions $^4I_{15/2}(0)\rightarrow{}^4I_{11/2}(0'\ldots5')$ and $^4I_{15/2}(0)\rightarrow{}^4I_{9/2}(0'\ldots4')$. The assignments of crystal-field levels and energies of the states used in the discussion are taken from Ref. 5 and collected in Table I.

Although the energy gaps between the various multiplets of Er^{3+} are small, multiphonon relaxation is not competitive for most of them in $Cs_3Er_2Br_9$ and $Cs_3Lu_2Br_9$:1%Er^{3+} due to the very low phonon energies of ≤ 190 cm^{-1}.[2] Compared to high-phonon systems such as oxides and fluorides this leads to completely different intensity distributions in the luminescence spectra. As shown in Fig. 5, the excited states $^4F_{7/2}$ and $^2H_{9/2}$ are not quenched by multiphonon relaxation at 10 K in $Cs_3Lu_2Br_9$:1%Er^{3+} and relax radiatively.

Besides the low phonon energy also the concentration of Er^{3+} doped into $Cs_3Lu_2Br_9$ strongly affects relative luminescence intensities. This is shown in Fig. 4 where the dominant $^4F_{7/2}\rightarrow{}^4I_{15/2}$ transition in

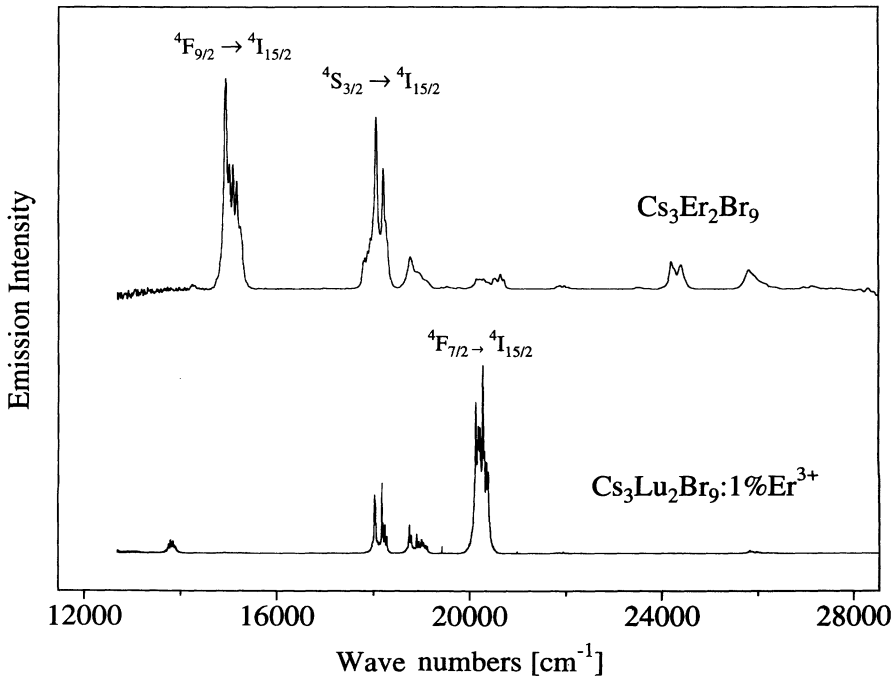

FIG. 4. Unpolarized upconversion luminescence spectra of $Cs_3Er_2Br_9$ and $Cs_3Lu_2Br_9$:1%Er^{3+} at room temperature using continuous-wave (CW) $^4I_{11/2}$ excitation. The intensity scale of the spectra is different.

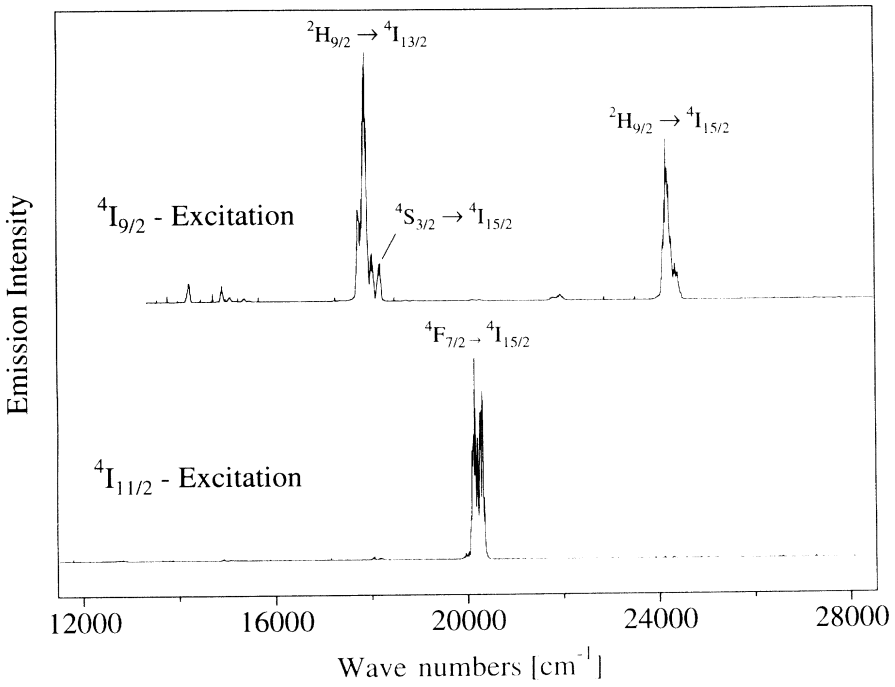

FIG. 5. Unpolarized upconversion luminescence spectra of $Cs_3Lu_2Br_9$:1%Er^{3+} at 10 K using pulsed excitation of $^4I_{9/2}$ and $^4I_{11/2}$, respectively. The intensity scale of the spectra is different.

$Cs_3Lu_2Br_9$:1%Er^{3+} is seen to be almost completely quenched in $Cs_3Er_2Br_9$ at room temperature. This quenching arises from additional efficient cross-relaxation processes from $^4F_{7/2}$ which are suppressed in the diluted system.[4] Due to the suppression of a variety of relaxation pathways in the diluted system, relatively pure upconversion luminescence from $^4F_{7/2}$ and $^2H_{9/2}$ is observed after pulsed or CW excitation of $^4I_{11/2}$ and $^4I_{9/2}$, respectively. $Cs_3Lu_2Br_9$:1%Er^{3+} is therefore an ideal system for the study of the dynamics of NIR-to-VIS upconversion, and especially the first upconversion step can be investigated in detail.

B. Radiative relaxation

As multiphonon relaxation and cross-relaxation processes are strongly suppressed in $Cs_3Lu_2Br_9$:1%Er^{3+} up to room temperature, rate constants for radiative relaxation are experimentally accessible by direct excitation for some of the relevant excited states.[4] The lifetimes in

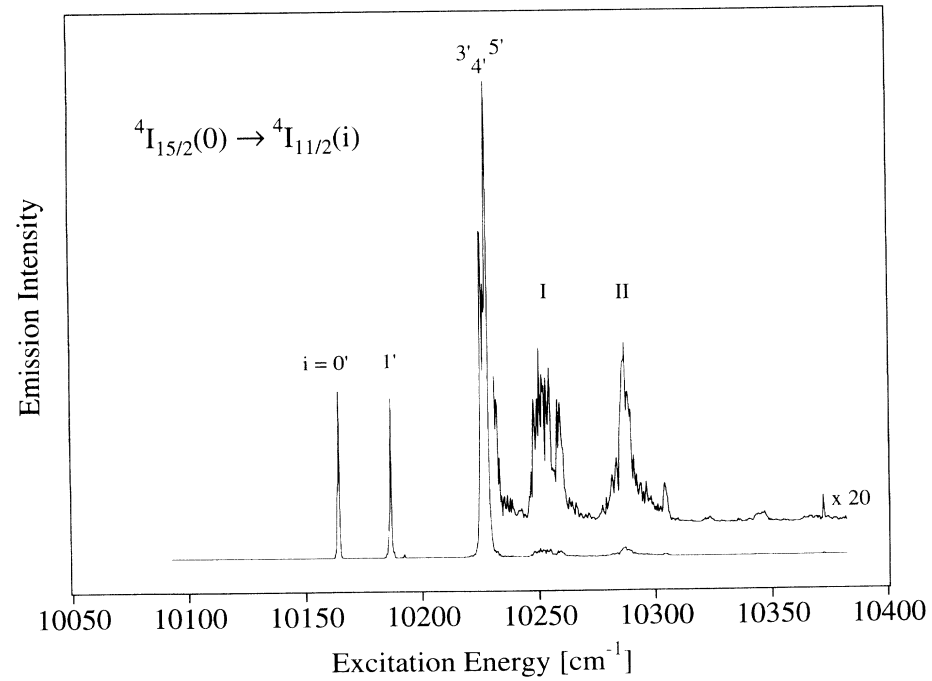

FIG. 6. Pulsed $^4I_{15/2} \rightarrow {}^4I_{11/2}$ excitation spectrum of $Cs_3Lu_2Br_9$:1%Er^{3+} at 10 K monitoring the $^4F_{7/2} \rightarrow {}^4I_{15/2}$ upconversion luminescence. The labels $^4I_{11/2}(i)$ $(i = 0' \ldots 5')$ denote crystal-field levels (see Table I), I and II denote two additional bands referred to in the text.

$Cs_3Lu_2Br_9$:1%Er^{3+} (see Table II) are similar to those found in $CsCdBr_3$:Er^{3+} in which the coordination geometry and the multiphonon relaxation properties are comparable to $Cs_3Lu_2Br_9$:1%Er^{3+}.[3] In particular, we note the long lifetimes of $^4F_{7/2}$ and $^4F_{5/2}$, states which are efficiently quenched by multiphonon relaxation in oxide and fluoride host lattices. In $Cs_3Lu_2Br_9$:1%Er^{3+} the lifetimes are almost temperature independent between 10 and 300 K. This is another reflection of the unimportance of multiphonon relaxation in this host.

C. Radiative versus nonradiative upconversion

In principle, upconversion can occur by two different mechanisms, radiatively by an excited-state absorption (ESA) or nonradiatively by an energy transfer (ETU) after excitation. Although there is a resonance condition for both processes, perfect resonance between the involved transitions is very rare. This is mainly due to the very small linewidth of electronic *4f* transitions. Possible small energy mismatches are compensated by the absorption or emission of phonons.

Using CW excitation it is not possible to directly distinguish between ESA and ETU processes. This is different in a pulsed experiment with an excitation pulse width δt in the ns range or below. The radiative ESA process occurs within δt, whereas nonradiative ETU can also proceed after the excitation pulse. Referring to Fig. 1, upconversion to state $|3\rangle$ can still proceed by ETU after excitation into $|2\rangle$, but both steps of the ESA process $|1\rangle \rightarrow |2\rangle \rightarrow |3\rangle$ have to take place within the time δt. This directly affects the upconversion transient $N_3(t)$. If $|3\rangle$ is solely populated by ETU, $N_3(t)$ consists of a rise and a decay which are determined by the relaxation rate constants of the states involved and the energy-transfer

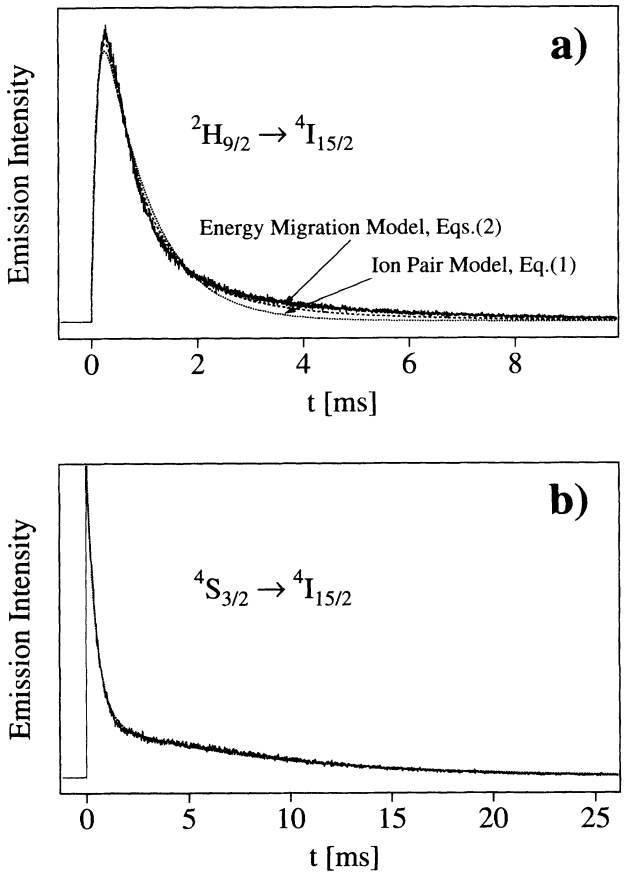

FIG. 7. (a) $^2H_{9/2} \rightarrow {}^4I_{15/2}$ and (b) $^4S_{3/2} \rightarrow {}^4I_{15/2}$ upconversion transients under $^4I_{9/2}$ excitation of $Cs_3Lu_2Br_9$:1%Er^{3+} at 10 K. The excitation pulse has a width of 10 ns and occurs at $t=0$. The calculated curves are described in Sec. V D.

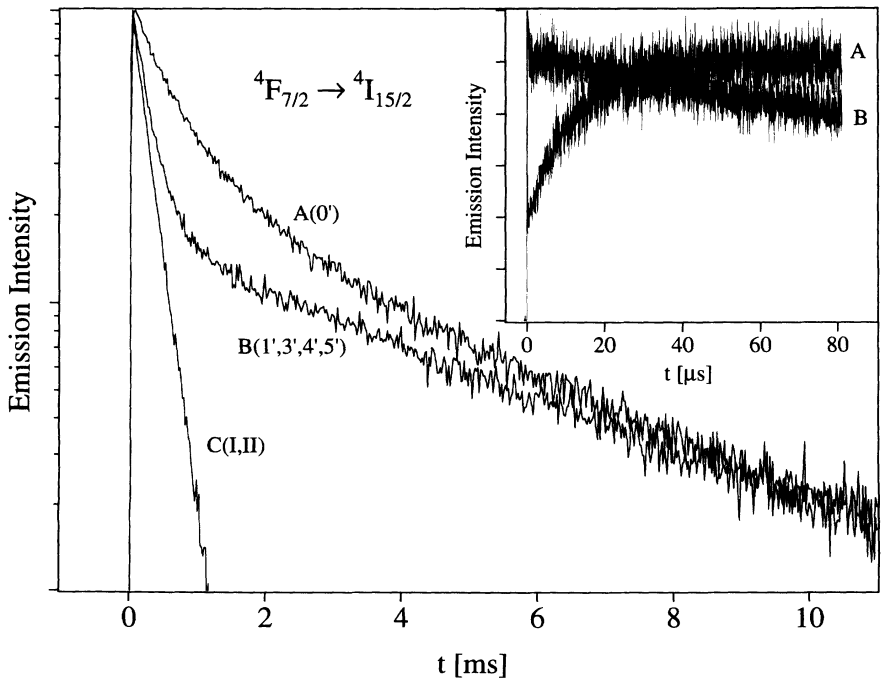

FIG. 8. $^4F_{7/2} \rightarrow {}^4I_{15/2}$ upconversion transients under $^4I_{11/2}$ excitation of $Cs_3Lu_2Br_9$:1%Er^{3+} at 10 K. The intensity maxima of the transients are normalized and the ordinate scale is logarithmic. The excitation pulse has a width of 10 ns and occurs at $t=0$. The transients *A*, *B*, *C* are recorded using different excitation energies, the labels given in parentheses refer to Fig. 6. The inset shows the transients *A* and *B* for short times after the excitation pulse on a linear ordinate scale.

TABLE II. Lifetimes τ of some relevant excited states in $Cs_3Lu_2Br_9$:1%Er^{3+} (10 and 300 K) and $CsCdBr_3$:1%Er^{3+} (10 K) (from Ref. 3). The lifetimes in $Cs_3Lu_2Br_9$:1%Er^{3+} were obtained by direct excitation of the respective excited states.

	$Cs_3Lu_2Br_9$:1%Er^{3+}		$CsCdBr_3$:Er^{3+}
Multiplet	τ (ms) (T=10 K)	τ (ms) (T=300 K)	τ (ms) (T=10 K)
$^4I_{13/2}$	9.0	6.3	
$^4I_{11/2}$	11.0		12.8
$^4I_{9/2}$	8.0		11.1
$^4S_{3/2}$	0.333	0.264	
$^2H_{11/2}$	0.004	0.0007	
$^4F_{7/2}$	0.232	0.258	0.210
$^4F_{5/2}$	0.428	0.418	
$^2H_{9/2}$			0.266

rate constant (see Sec. III). This is different for an ESA upconversion process. $|3\rangle$ is populated within the time δt, i.e., within the time resolution of the experiment; it subsequently decays with its relaxation constant. As the time constants which are involved in ETU processes are usually significantly longer than $\delta t \approx 10$ ns, the observation of population N_3 within δt is a direct indication for an ESA process. This is nicely illustrated in Figs. 7(a) and 7(b). Whereas $^2H_{9/2}$ is populated by an ETU process after the laser pulse [Fig. 7(a)], the maximum of $^4S_{3/2}$ population is reached within δt, clearly indicating an ESA process [Fig. 7(b)]. We can thus use the rise of the upconversion transient as a fingerprint for the nature of the active upconversion process.

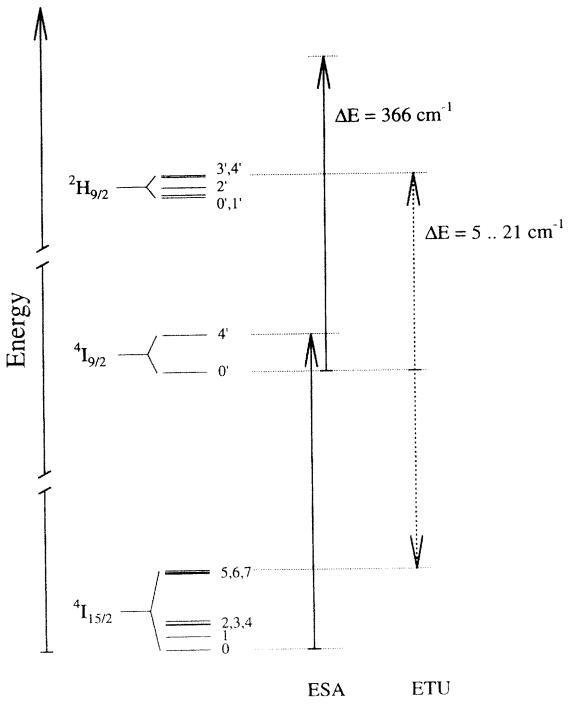

FIG. 9. Schematic representation of the resonances for $^4I_{9/2}(0')+h\nu \rightarrow {}^2H_{9/2}(3',4')$ excited-state absorption (ESA) and $^4I_{9/2}(0'),{}^4I_{9/2}(0') \rightarrow {}^4I_{15/2}(5,6,7),{}^2H_{9/2}(3',4')$ energy-transfer upconversion (ETU) in $Cs_3Lu_2Br_9$:1%Er^{3+} for $^4I_{15/2}(0) \rightarrow {}^4I_{9/2}(4')$ excitation. The energy differences ΔE for both mechanisms were calculated from the crystal-field energies given in Table I.

D. $^4I_{9/2}$ excitation: Upconversion mechanisms

The possible processes for upconversion of $^4I_{9/2}$ excitation to $^2H_{9/2}$ are shown in Fig. 9. In a first step, the system is excited to the $^4I_{9/2}(4')$ level at 12 476 cm^{-1}. The subsequent thermalization of the $^4I_{9/2}$ excited state takes place on a ps time scale and is thus significantly shorter than the duration of the laser pulse ($\delta t = 10$ ns). For this reason, the initial level for the second excitation step is $^4I_{9/2}(0')$ (T=10 K) regardless of the nature of the following upconversion process. Figure 9 shows the relevant energy differences for the second step for both mechanisms ESA and ETU. Whereas the ETU processes

$$^4I_{9/2}(0'),{}^4I_{9/2}(0') \rightarrow {}^4I_{15/2}(5,6,7),{}^2H_{9/2}(3',4')$$

are almost resonant, the ESA processes on a single ion,

$$^4I_{9/2}(0')+h\nu \rightarrow {}^2H_{9/2}(3',4') ,$$

are off-resonant by at least +366 cm^{-1} for the given excitation energy ($h\nu$=12 476 cm^{-1}). Therefore, ESA is not likely to occur, and ETU is expected to be the dominant upconversion mechanism for $^4I_{9/2}$ excitation. This is confirmed by the $^2H_{9/2}$ transient shown in Fig. 7(a). From the considerations presented in Sec. V C, ESA can be excluded as no $^2H_{9/2}$ population is created during the laser pulse. Rather the $^2H_{9/2}$ transient has a shape typical for ETU (see Sec. III). We conclude that in $Cs_3Lu_2Br_9$:1%Er^{3+} $^4I_{9/2}$ upconversion to $^2H_{9/2}$ cannot occur on an isolated Er^{3+} ion and at least two excited ions in close proximity are required to populate $^2H_{9/2}$ by ETU.

We assume the Er^{3+} ions doped into the host lattice $Cs_3Lu_2Br_9$ to be distributed statistically. The lattice consists of close $[Lu_2Br_9]^{3-}$ dimer units with a Lu^{3+}-Lu^{3+} separation of only 3.9 Å.[13] Due to this short ion-ion separation the intradimer coupling is strong,[14] and energy-transfer processes within these dimers are expected to be very efficient. Neighboring dimers are separated by 5.8–8.3 Å so that interdimer energy transfer has to be considered as well. Besides Er^{3+} in the crystallographic dimer units a variety of interdimer ion pairs also provide ETU pathways. With increasing Er^{3+} concentration the upconversion properties are therefore expected to change from being ion-pair to energy-migration dominated.

Figure 7(a) shows fits to the $^2H_{9/2}$ transient for both ETU models presented in Sec. III. The isolated ion-pair model [Eq. (1)] yields a rise and a decay rate constant of 9733 and 1134 s^{-1}, respectively. Whereas the experimental rise of the $^2H_{9/2}$ transient is well reproduced, this model is not able to reproduce the long decay part of the transient. Neither the rise nor the decay rate constant is comparable to the $^2H_{9/2}$ relaxation rate constant of 3760 s^{-1} derived for $CsCdBr_3$:Er^{3+}.[3] A different and much better result is obtained from the energy migration model [Eqs. (2)], see Fig. 7(a). Using the $^4I_{9/2}$ relaxation rate constant W_2=125 s^{-1} from Table II, this model yields

the rate constants $W_t = 792\ s^{-1}$ and $W_3 = 6161\ s^{-1}$. The fast rise of the $^2H_{9/2}$ transient is thus correlated to the fast decay of $^2H_{9/2}$, and the decay of the transient reflects the relaxation of the $^4I_{9/2}$ ETU initial state. We conclude that the isolated ion-pair model is not adequate for the description of $^4I_{9/2} \rightarrow {}^2H_{9/2}$ ETU in $Cs_3Lu_2Br_9$:1%Er^{3+}, and efficient energy migration is active already at the doping level of 1% Er^{3+}. This result is confirmed by experiments in YF_3:Yb^{3+},Ho^{3+} where energy migration among Yb^{3+} ions was found to be noticeable at 0.3% and dominant above 3% Yb^{3+}.[15]

The value $W_t = 792\ s^{-1}$ which is obtained from the fit of the energy-migration model [see Fig. 7(a)] is significantly smaller than the value 1741 s^{-1} reported for the corresponding pair process in $CsCdBr_3$:Er^{3+}.[3] Assuming a statistical distribution in 1% Er^{3+} doped $Cs_3Lu_2Br_9$ 85% of the Er^{3+} ions do not have an Er^{3+} neighbor within 10 Å, a distance at which energy transfer is still efficient. The relevant average Er^{3+}-Er^{3+} separation is therefore larger than the 6.0 Å for the dominant Er^{3+}-vacancy-Er^{3+} center in $CsCdBr_3$:Er^{3+}. This could account for the lower value for W_t found in $Cs_3Lu_2Br_9$:1%Er^{3+}.

Besides the dominant upconversion luminescence from $^2H_{9/2}$ also weak luminescence from $^4S_{3/2}$ is observed under $^4I_{9/2}$ excitation (see Fig. 5). The $^4S_{3/2}$ transient is shown in Fig. 7(b) and is very different from the $^2H_{9/2}$ transient [see Fig. 7(a)]. The decay consists of two distinct parts, a fast component and a slow decay which bears most of the intensity. In contrast to $^2H_{9/2}$ the rise of the $^4S_{3/2}$ luminescence intensity is instantaneous. Figure 10 shows two possible processes on an ion pair which could lead to $^4S_{3/2}$ population within δt: (i) After a first $^4I_{15/2} \rightarrow {}^4I_{9/2}$ excitation, a doubly excited $^4I_{9/2}$,$^4I_{9/2}$ ion pair is formed due to either a second absorption or the efficient energy migration. From the $^4I_{9/2}$,$^4I_{9/2}$ doubly excited ion pair, $^4S_{3/2}$,$^4I_{13/2}$ can be populated by an energy-transfer process whose time constant has to be comparable to δt. (ii) After a first $^4I_{15/2} \rightarrow {}^4I_{9/2}$ excitation, a second photon is absorbed in a cooperative ESA on an ion pair. From the crystal-field energies (see Table I) the cooperative ESA process

$$^4I_{15/2}(0), {}^4I_{9/2}(0') + h\nu \rightarrow {}^4I_{13/2}(3'), {}^4S_{3/2}(1')$$

is found to be resonant ($\Delta E = -1\ cm^{-1}$) within the experimental accuracy for the excitation energy $h\nu = 12\,476\ cm^{-1}$. On the basis of Sec. V C, we assign process (ii), the cooperative ESA on an ion pair, to the active mechanism responsible for the $^4S_{3/2}$ population within δt. The nonresonant energy transfer (i)

$$^4I_{9/2}(0'), {}^4I_{9/2}(0') \rightarrow {}^4I_{13/2}(0') {}^4S_{3/2}(0')$$

($\Delta E = -28\ cm^{-1}$, see Fig. 10) is a "bottleneck" and occurs with a time constant much longer than δt. This is the ETU mechanism which leads to the $^4S_{3/2}$ population at longer times. Two types of Er^{3+} ions are responsible for the observed $^4S_{3/2} \rightarrow {}^4I_{15/2}$ transient: Those who have reached the $^4S_{3/2}$ state by cooperative ESA and those who have reached it by ETU. As the cooperative ESA process (ii) proposed above is selective only for the minority of Er^{3+} ions in close proximity its induced $^4S_{3/2}$ intensity is low compared to the $^4S_{3/2}$ intensity induced by the ETU process (i) [see Fig. 7(b)].

The dotted line in Fig. 7(b) is a fit of the energy-transfer model [Eqs. (2)] presented in Sec. III. An initial $^4S_{3/2}$ population is included as an additional parameter to account for those Er^{3+} ions which have reached the $^4S_{3/2}$ state by cooperative ESA. The transient is nicely reproduced, and the fit yields a $^4S_{3/2}$ decay time constant of 463 μs which is reasonably close to the value of 333 μs determined by direct excitation (see Table II). For the relaxation of $^4I_{9/2}$ a rate constant of $W_2 = 61\ s^{-1}$ is obtained from the fit of Eqs. (2). This low $^4I_{9/2}$ relaxation rate constant leads to the long observed decay of the $^4S_{3/2}$ transient [Fig. 7(b)] in analogy to the $^2H_{9/2}$ transient discussed above.

As is evident from both transients $^2H_{9/2}$ [Fig. 7(a)] and $^4S_{3/2}$ [Fig. 7(b)] and the numbers extracted from the model fits, the long decay constants are different although they were both assigned to the decay of $^4I_{9/2}$. Whereas the $^2H_{9/2}$ transient could be reproduced using the experimentally found value $W_2 = 125\ s^{-1}$ (Table II) the fit of Eqs. (2) to the $^4S_{3/2}$ transient gives a relaxation rate constant $W_2 = 61\ s^{-1}$. This discrepancy suggests that the two upconversion luminescences arise from different ion clusters in the lattice. This conclusion is further supported by the relative luminescence intensities from $^2H_{9/2}$ and $^4S_{3/2}$ (see Fig. 5). Although the ETU processes populating $^2H_{9/2}$ and $^4S_{3/2}$ are very similar with respect to their energetic resonance (see Figs. 9 and 10) and are therefore expected to have comparable rate constants, the populations they create differ by at least an order of magnitude (see Fig. 5).

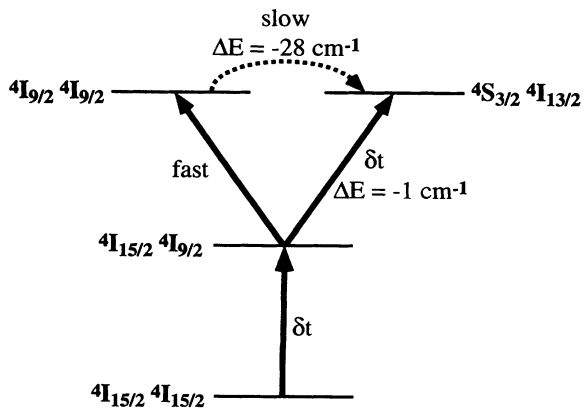

FIG. 10. Schematic representation of excitation mechanisms for $^4S_{3/2}$ upconversion luminescence. The energy differences ΔE were calculated from the crystal-field energies given in Table I. The processes are described in Sec. V D.

E. $^4I_{11/2}$ excitation: Upconversion mechanisms

Using $^4I_{11/2}$ excitation, upconversion luminescence from $^4F_{7/2}$ is dominant at 10 K (see Fig. 5). Exciting different crystal-field levels within the $^4I_{11/2}$ multiplet (see Fig. 6) results in very different behavior of the $^4F_{7/2}$

transients shown in Fig. 8. This is a rather striking effect which has not been described before. In our view it is clear evidence for the presence of two competing upconversion mechanisms. Depending on the excitation energy two different $^4F_{7/2}$ decay constants of about 270 μs and 5 ms are observed which roughly correspond to the $^4F_{7/2}$ and $^4I_{11/2}$ lifetimes, respectively (see Table II). After any $^4I_{15/2} \rightarrow {}^4I_{11/2}(0' \ldots 5')$ excitation very fast thermalization processes lead to the same $^4I_{11/2}(0')$ initial level ($T = 10$ K) for all further upconversion steps. Therefore no dependence of the $^4F_{7/2}$ transient on the initially excited $^4I_{11/2}$ crystal-field level is expected for ETU, and we therefore have to consider additional excitation mechanisms.

Figure 11 shows the energetic situation for $^4I_{11/2}$ upconversion for the excitation energies used to obtain Fig. 8. In contrast to $^4I_{9/2}$ upconversion (see Sec. V D), the resonances for ETU and ESA are comparable and both processes have to be considered for upconversion. All ETU processes are off-resonant by at least $\Delta E = -18$ cm^{-1} and thus can only occur by phonon assistance. For the ESA processes we distinguish three types of excitation energies *A* ($h\nu = 10\,164$ cm^{-1}), *B* ($h\nu = 10\,187$ or $10\,228$ cm^{-1}), *C* ($h\nu = 10\,250$ or $10\,287$ cm^{-1}) with increasing degrees of resonance (see Fig. 11): *A* has $\Delta E = -18$ cm^{-1}, *B* is almost resonant for ESA, and *C* exactly matches within the experimental accuracy. These three types of excitation lead to the distinct rise and decay characteristics of the $^4F_{7/2}$ transients shown in Fig. 8. There is clearly a competition between ESA and ETU. Depending on the excitation energy, both $^4I_{11/2}$ and $^4F_{7/2}$ (by ESA) are populated during the laser pulse. The relative population of $^4I_{11/2}$ is a maximum for excitation *A* where the resonance for ESA is worst. This is seen in the rise of transient *A* (see the inset of Fig. 8) which consists of both an initial intensity due to ESA and a slow population after the laser pulse due to ETU. For excitation *B* and especially for *C*, ESA is strongly favored. In the case of *C* no measurable population is left in $^4I_{11/2}$, and the $^4F_{7/2}$ transient is similar to one using direct excitation of $^4F_{7/2}$.

As shown in Fig. 11 excitation *C* is resonant with the $^4I_{11/2}(0') + h\nu \rightarrow {}^4F_{7/2}(2',3')$ ESA and off-resonant for any $^4I_{15/2} \rightarrow {}^4I_{11/2}(0' \ldots 5')$ ground-state absorption. Therefore, the first excitation step is very inefficient for excitation energy *C*, and it can only take place by an absorption into a vibrational sideband of $^4I_{11/2}$. When ESA is resonant, as is the case for excitation *C*, the population created by this weak $^4I_{15/2} \rightarrow {}^4I_{11/2}$ absorption is efficiently upconverted. This is the origin of bands I and II in Fig. 6 which arise from the ESA resonances $^4I_{11/2}(0') + h\nu \rightarrow {}^4F_{7/2}(2')$ ($h\nu = 10\,250$ cm^{-1}) and $^4I_{11/2}(0') + h\nu \rightarrow {}^4F_{7/2}(3')$ ($h\nu = 10\,287$ cm^{-1}), respectively. With a full width of about 14 cm^{-1} and 24 cm^{-1} both bands I and II are significantly broader than the other crystal-field transitions shown in Fig. 6. For both bands I and II, the peak intensity is found in the center region of the band (see Fig. 6) indicating the energies where ESA is exactly resonant. Therefore, the half widths of the bands of approximately 7–12 cm^{-1} roughly indicate the maximum off-resonance for an ESA process to be still efficient within the 10 ns of the laser pulse. This is an energetic rule for estimating the efficiency of an ESA process. In Fig. 11, this rule is confirmed: Excitations *B* and *C* are within a maximum off-resonance of 7–12 cm^{-1} and lead to efficient ESA. This is in contrast to excitation *A* (off-resonance 18 cm^{-1}) which has a substantially lower ESA efficiency (see the inset in Fig. 8).

Bands I and II provide further information on the nature of the ESA process. In Fig. 6, an asymmetric intensity distribution is observed for both bands, i.e., more intensity is found for energies greater than the respective band maximum. For these excitation energies phonons are created during the ESA process and released to the

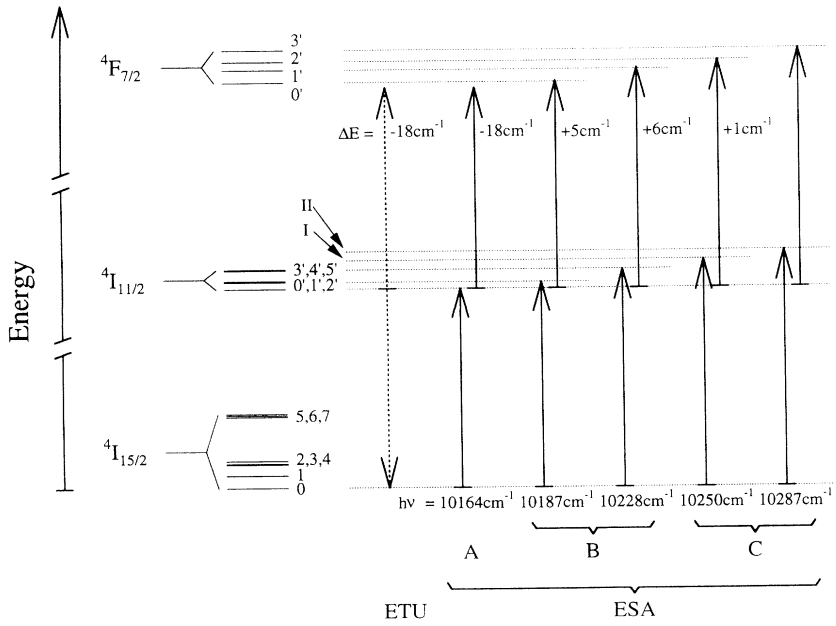

FIG. 11. Schematic representation of the resonances for $^4I_{11/2} + h\nu \rightarrow {}^4F_{7/2}$ excited-state absorption (ESA) and $^4I_{11/2}, {}^4I_{11/2} \rightarrow {}^4I_{15/2}, {}^4F_{7/2}$ energy-transfer upconversion (ETU) in $Cs_3Lu_2Br_9$:1%Er^{3+}. The energy differences ΔE for both mechanisms were calculated from the crystal-field energies given in Table I. The excitation energies $h\nu$ for the different ESA processes are included in the figure. The labels *A*, *B*, *C* refer to the different types of transients shown in Fig. 8. The processes are described in Sec. V E.

lattice. For energies below the band maximum an ESA can only take place by the simultaneous absorption of lattice phonons. Whereas the emission of phonons during the ESA process is temperature independent, the phonon absorption crucially relies on the phonon density. At 10 K high-energy phonons are very rare and thus ESA processes for energies below resonance are very unlikely. This induces an asymmetry which is observed in bands I and II and which is expected to vanish at higher temperatures. In Fig. 6, we further note that the two bands, I and II, have a different and very complex structure. This is determined by both the phonon density and the individual electron-phonon coupling of the involved transitions.

Finally, we note a nice confirmation of these results by a crystal-field calculation for this system.[5] The crystal-field level $^4F_{7/2}(3')$ could not be observed in the absorption experiments. The right-most process shown in Fig. 11 predicts a $^4F_{7/2}(3')$ energy of 20 451 cm^{-1} assuming exact resonance for the ESA. This is almost identical with the calculated value of 20 450 cm^{-1} (Ref. 5) and confirms the assignment of band II in Fig. 6.

VI. CONCLUSIONS

The temporal behavior of NIR-to-VIS upconversion in $Cs_3Lu_2Br_9$:1%Er^{3+} is well accounted for by a pair model and, alternatively, by a model which assumes efficient energy migration among the Er^{3+} ions. An analysis of the $^2H_{9/2}$ transient could directly exclude upconversion originating from isolated ion pairs. Both excited-state absorption (ESA) and energy-transfer upconversion (ETU) are observed and can unambiguously be identified on the basis of the upconversion transients. A resonance criterion for the efficiency of ESA and ETU processes could be formulated on the basis of both the time-resolved upconversion measurements and the detailed knowledge of the energy-level structure of this system. Whereas ESA is strongly suppressed during the 10-ns laser pulse if the off-resonance is greater than about 12 cm^{-1}, ETU is still efficient for much larger energy mismatches. As efficient upconversion is required, e.g., in upconversion laser systems, this resonance criterion is essential to optimize a desired pumping scheme. Time-resolved upconversion spectroscopy in $Cs_3Lu_2Br_9$:1%Er^{3+} has shown to be a powerful tool to gain insight into the dynamics of upconversion. The transients are a fingerprint of both the nature of the upconverting centers and the active upconversion processes.

ACKNOWLEDGMENTS

We thank A. Hauser for valuable discussions. Financial support by the Swiss National Science Foundation is gratefully acknowledged.

*Present address: Los Alamos National Laboratory, Chemical Science and Technology Division, Mailstop E535, Los Alamos, NM 87545.

[1]K. Krämer and H. U. Güdel, J. Alloys Compounds **207/208**, 128 (1994).

[2]M. P. Hehlen, K. Krämer, H. U. Güdel, R. A. McFarlane, and R. N. Schwartz, Phys. Rev. B **49**, 12 475 (1994).

[3]N. J. Cockroft, G. D. Jones, and D. C. Nguyen, Phys. Rev. B **45**, 5187 (1992).

[4]M. P. Hehlen, K. Krämer, and H. U. Güdel, J. Lumin. **60&61**, 142 (1994).

[5]M. P. Hehlen, H. U. Güdel, and J. R. Quagliano, J. Chem. Phys. (to be published).

[6]G. Meyer, *Synthesis of Lanthanide and Actinide Compounds* (Kluwer Academic, Dordrecht, 1991).

[7]F. Auzel, Proc. IEEE **61**, 758 (1973).

[8]J. C. Wright, in *Radiationless Processes in Molecules and Condensed Phases,* edited by F. K. Fong, Topics in Applied Physics Vol. 15 (Springer-Verlag, Berlin, 1976).

[9]F. Auzel, J. Lumin. **45**, 341 (1990).

[10]D. L. Dexter, J. Chem. Phys. **21**, 836 (1953).

[11]L. M. Henling and G. L. McPherson, Phys. Rev. B **16**, 4756 (1977).

[12]R. Buisson and J. C. Vial, J. Phys. (Paris) Lett. **42**, L115 (1981).

[13]G. Meyer, Prog. Solid State Chem. **14**, 141 (1982).

[14]H. U. Güdel, A. Furrer, and H. Blank, Inorg. Chem. **29**, 4081 (1990).

[15]R. K. Watts and H. J. Richter, Phys. Rev. B **6**, 1584 (1972).